Implications of Mitigating Ozone and Fine Particulate Matter Pollution in the Greater Bay Area Using a Regional-to-Local Coupling Model

Xuguo Zhang[1,2], Jenny Stocker[3], Kate Johnson[3], Yik Him Fung[2], Teng Yao[2], Christina Hood[3], David Carruthers[3], and Jimmy C. H. Fung[1,2,*]

[1] Department of Mathematics, The Hong Kong University of Science and Technology, Hong Kong.

[2] Division of Environment and Sustainability, The Hong Kong University of Science and Technology, Hong Kong.

[3] Cambridge Environmental Research Consultants, Cambridge, UK.

Corresponding author: Jimmy C. H. Fung (majfung@ust.hk)

Key Points:

- A regional-to-local coupled model is constructed to explore the likely impact of emissions reductions and pollution mitigation pathways.
- The O_3 formation regime in Guangzhou is VOC-limited and the traffic sector is of paramount importance for controlling NO_x and O_3.
- Investigation of frequent summer O_3 episodes emphasizes the value of more stringent VOC controls, particularly for the industrial sector.

ORCID: 0000-0001-7857-2525 (X. Zhang); 0000-0003-3243-7226 (J. Stocker); 0000-0002-7071-1137 (Y.H. Fung); 0000-0001-9244-5696 (C. Hood); 0000-0002-7859-8511 (J.C.H. Fung)

Abstract

Ultrahigh-resolution air quality models that resolve sharp gradients of pollutant concentrations benefit the assessment of human health impacts. Mitigating fine particulate matter ($PM_{2.5}$) concentrations over the past decade has triggered ozone (O_3) deterioration in China. Effective control of both pollutants remains poorly understood from an ultrahigh-resolution perspective. We propose a regional-to-local model suitable for quantitatively mitigating pollution pathways at various resolutions. Sensitivity scenarios for controlling nitrogen oxide (NO_x) and volatile organic compound (VOC) emissions are explored, focusing on traffic and industrial sectors. The results show that concurrent controls on both sectors lead to reductions of 17%, 5%, and 47% in NO_x, $PM_{2.5}$, and VOC emissions, respectively. The reduced traffic scenario leads to reduced NO_2 and $PM_{2.5}$, but increased O_3 concentrations in urban areas. Guangzhou is located in a VOC-limited O_3 formation regime, and traffic is a key factor in controlling NO_x and O_3. The reduced industrial VOC scenario leads to reduced O_3 concentrations throughout the mitigation domain. The maximum decrease in median hourly NO_2 is >11 µg/m³, and the maximum increase in the median daily maximum 8-hour rolling O_3 is >10 µg/m³ for the reduced traffic scenario. When controls on both sectors are applied, the O_3 increase reduces to <7 µg/m³. The daily averaged $PM_{2.5}$ decreases by <2 µg/m³ for the reduced traffic scenario and varies little for the reduced industrial VOC scenario. An O_3 episode analysis of the dual-control scenario leads to O_3 decreases of up to 15 µg/m³ (8-h metric) and 25 µg/m³ (1-h metric) in rural areas.

Plain Language Summary

Spatial concentration maps of air pollutants showing variations over small distances are useful for assessing human health in metropolitan regions. The combined control of fine particulate matter and ozone is not yet fully understood at a high resolution. This study implements a regional-to-local urban modeling system for quantitatively assessing opportunities for pollution reduction. Typical air pollutants are explored, focusing on emissions from the traffic and industrial sectors. We find that implementing combined controls in both sectors leads to considerable reductions in emissions. Scenario analysis reveals the most substantial contributors to ozone pollution in various locations. The contributions of air pollution from both sectors are assessed. The research findings will improve the awareness of air quality management strategies and benefit multi-level governments by facilitating joint control of regional air pollution issues.

Index Terms

3355 Regional modeling (4316); 0345 Pollution: urban and regional (0305, 0478, 4251, 4325); 0545 Modeling (1952, 4255, 4316); 3329 Mesoscale meteorology; 6620 Science policy (0485, 4338).

Keywords

street-scale; air dispersion model; CMAQ–ADMS-Urban; sensitivity analysis; ozone; Greater Bay Area.

1 Introduction

Air pollution has attracted substantial research interests in recent years owing to its adverse effects on human health (Che et al., 2020; Conibear et al., 2021; Wu et al., 2019) and climate change (Li et al., 2019c; Qin et al., 2017). Since President Xi announced a bold pledge that Chinese carbon emissions would peak before 2030 and China would achieve carbon neutrality by 2060, greater efforts have been made to alleviate air pollution (Cheng et al., 2021; Cui et al., 2021). The Chinese government has devoted tremendous efforts and released a series of emissions control policies to address this challenge (Cai et al., 2018; Jiang et al., 2015; Wu et al., 2019; Zhang et al., 2020). Zhang et al. (2020) proposed a holistic emissions control system that utilized a chemical transport model method to assess the impacts of the implemented emissions control policies in various sectors during the 13th Five-Year-Plan in China. In response to stringent national controls, ambient fine particulate matter ($PM_{2.5}$) pollution has decreased substantially, whereas ozone (O_3) pollution levels are becoming increasingly severe (Li et al., 2019b; Zhao et al., 2021). The combined impact of $PM_{2.5}$ and O_3 on human health has improved over the past decade (Zhang et al., 2021a); however, high O_3 concentrations have an adverse effect on ecosystems (Yli-Pelkonen et al., 2017), so long-term controls of atmospheric O_3 are necessary. As such, strategies for effectively controlling the absolute concentrations of O_3 and $PM_{2.5}$ simultaneously in urban regions are of increasing interest and importance.

A growing number of studies have devoted great efforts to the mechanism of coupled O_3 and $PM_{2.5}$ pollution levels in regions throughout China. Li et al. (2019a) found that the main cause of increasing O_3 concentrations in the North China Plain (NCP) after 2013 was a significant reduction in $PM_{2.5}$ concentrations, which slowed hydroperoxy radical consumption and increased the rate of O_3 formation. Zhao et al. (2021) confirmed the interactions between the two pollutants and called for their concurrent control following an analysis of 4-year observational data in China. Li et al. (2019b) proposed aggressive reductions of nitrogen oxide (NO_x) and volatile organic compound (VOC) emissions to control air pollution in the NCP following analysis of summer O_3 surface data collected during 2013–2018. Gong et al. (2021) utilized the Community Multiscale Air Quality (CMAQ) model at a 12-km resolution to trace the precursors of $PM_{2.5}$ and O_3; exploring the regional effects of pollution transport on the interaction among the $PM_{2.5}$ and O_3 from cities in the Yangtze River Delta (YRD) region. In addition, using the same CMAQ model, Li et al. (2021a) concluded that industrial and traffic emissions were the dominate sources of both pollutants in the YRD. These findings have motivated further studies on the impact of precursors NO_x and VOC emissions from traffic and industrial sources in China.

Other studies have focused on quantifying the effects of model resolutions on air pollution simulations and health risks. A study conducted in the United States proved that a CMAQ model with finer resolution (4-km versus 12-km grid spacing) was better for estimating the effects on health in urban areas; the results for rural areas were comparable for both 4 and 12 km resolutions (Jiang and Yoo, 2018). Tao et al. (2020) found that finer-resolution modeling could better capture and reproduce the temporal trends and magnitudes of meteorological conditions and air quality in Beijing. In contrast, a localized study indicated that grid resolution had little effect on $PM_{2.5}$ and O_3 simulations in the YRD (Wang et al., 2021). Liu et al. (2020) demonstrated that model resolution did not significantly improve predictions of $PM_{2.5}$ and daily maximum 8-hour O_3 in Nanjing. However, the spatial distributions of both pollutants were better captured by a finer resolution model, leading to a >20% difference in estimates of premature mortality due to O_3 exposure (Liu et al., 2020). The impact of model resolutions on pollutant simulations and estimates of health risks has varied across different cities and regions (urban or rural). Consequently, exploring whether higher-resolution modeling techniques benefit model simulations for highly urbanized cities is of particular interest.

Previous studies have typically used a coarse-resolution (>1 km) model and an observation-oriented method to explore pollution sources or estimate health impacts for O_3 and $PM_{2.5}$ in the coupled systems (Li et al., 2021b; Silver et al., 2020). One study (Silveira et al., 2019) summarized a large number of coupled regional-to-local models that have been applied in urban regions worldwide; however, model calculation algorithms and assumptions have varied widely among other studies. The regional-to-local scale coupling system used in the current study follows the approach introduced in Hood et al. (2018) and Stocker et al. (2012). In this system, double-counting of local emissions is avoided by deducting local urban-scale modeling of all emissions, represented as grid sources, from the regional modeling of all emissions before adding street-scale local modeling with explicit and gridded sources. We balance the additional high-resolution emissions in the local urban-scale model by using a corresponding negative amount of emissions at the same gridding as the regional CMAQ model to emulate the effects of removing such emissions from the regional model grid. The coupled modeling system redistributes emissions within each of the regional grids for the purpose of running the local urban-scale model. The local modeling of road sources in an Urban Atmospheric Dispersion Modelling System (ADMS-Urban) can include street canyon effects, which affect the predicted concentrations both inside and outside a canyon (Hood et al., 2021). In the ADMS model, the H/W ratio is considered in street canyons, where a street is flanked by buildings on both sides to form a canyon-like environment. The H/W ratio is defined as the average building height on both sides of the street canyon divided by the distance between the two sides. The ADMS-Urban street canyon module was designed to account for street canyons with higher H/W ratios than the popular Operational Street Pollution Model (OSPM) model, which was developed for H/W ratios around 1. Few studies have applied coupled regional and very high-resolution (street level) modeling techniques to investigate the traffic and industrial contributions to complex coupled O_3 and $PM_{2.5}$ issues through testing of emissions scenarios. A street-scale model that provides a detailed representation of the spatial variation of pollutant gradients has clear advantages in terms of calculating health exposure over previous studies that have applied regional or global models.

Although urban-scale models have been used to investigate air pollution interactions in megacities, very few coupled model systems based on an ADMS-Urban and CMAQ models have been applied in the metropolitan region of the Greater Bay Area (GBA). Zhang et al. (2015) integrated the CMAQ model with the CALifornia PUFF (CALPUFF) model to simulate the contribution of SO_2 concentrations from local emissions in the GBA region. A regional European Monitoring and Evaluation Program Unified Model for the UK (EMEP4UK) with a resolution of 5 km was coupled with ADMS-Urban to perform street-level air pollutant simulations in London (Hood et al., 2018). Although ADMS-Urban was applied within the Sixth-Ring Road area in Beijing to simulate various pollutants (Biggart et al., 2020), it was not coupled with a regional model; instead the background concentration levels were adapted directly from measurement data and were assumed to be distributed uniformly across the model domain. As a result, our study is the first localized regional-to-local scale model system that couples ADMS-Urban and CMAQ to assess the sensitivity of two pollutants to emissions from traffic and industrial sectors in the GBA. The motivation for targeting these two sectors is related to the importance of the O_3 precursors, VOC and NO_x, derived from the anthropogenic industrial and traffic sectors in the GBA, respectively. Consequently, assessing the impact of changes to emissions of NO_x (and hence NO_2) and VOCs is of particular interest. Section 2 of this paper describes the regional and local street-scale model configurations and the sensitivity scenarios. The regional and local model simulation results and the model performance of selected monitoring stations are discussed in section 3. Section 4 presents a discussion of the research findings, followed by the conclusions in section 5.

2 Research Methods

2.1 Model configuration

Figure S1 shows a research framework for the CMAQ–ADMS-Urban air quality modeling system. The street-scale resolution ADMS-Urban dispersion model was coupled with the regional CMAQ model using the ADMS-Urban Regional Model Link (ADMS-Urban RML) to investigate O_3 and $PM_{2.5}$ concentrations and the sensitivity of both pollutants to emissions from the traffic and industrial sectors. The ADMS-Urban RML is used to automatically prepare nested data from the regional model (CMAQ) and the meso-scale meteorological model (WRF) for the street-level ADMS-Urban model. ADMS-Urban inherits the concentration outputs from the CMAQ model as background concentrations at each modeled hour. Most of the slow reactions are considered by the CMAQ chemical reaction scheme. The ADMS-Urban model is specialized in capturing the fine concentration gradient and rapid chemical reactions when emissions are released from pollution sources, such as in traffic settings. Over time, the concentration gradient lowers; the CMAQ model can simulate regional transport and the associated chemical reactions. In addition to the CMAQ output, the following reaction sets are calculated by the ADMS-Urban model. For NO_x–O_3, the Generic Reaction Set (Malkin et al., 2016) is used with an extra reaction introduced, i.e., $2NO + O_2 \Rightarrow 2NO_2$. For sulfates, sulfur dioxide is oxidized to particulates via the reactions $2SO_2 + O_2 \Rightarrow 2SO_3$, $SO_3 + H_2O \Rightarrow H_2SO_4$, and $H_2SO_4 + 2NH_3 \Rightarrow (NH_4)_2SO_4$.

The regional CMAQ model applied in this study is the same as that used to assess holistic emission control policies (Zhang et al., 2020), combined health effects (Zhang et al., 2021a), and data assimilation of model bias corrections (Zhang et al., 2021b) in our previous publications. In terms of the regional model configuration, detailed settings are described in the aforementioned publications, and only key points are listed below. The Sparse Matrix Operations Kernels Emissions (SMOKE) model was used to process the localized bottom-up emission inventory, including industrial sources, mobile sources, power plants, residential sources, and marine sources in the GBA. The marine emissions were split into ocean going vessels, local vessels, and river vessels and were calculated using automatic identification system data. The emission inventory outside the GBA was adapted from Multi-resolution Emission (MEIC) data (Tong et al., 2020). As shown in Figure S2, four nested domains with resolutions of 27 km (D1), 9 km (D2), 3 km (D3), and 1 km (D4) were utilized for the regional CMAQ model, and Domain 5 (6 km × 6 km), in an urban area of Guangzhou City, was chosen to drive the street-level ADMS-Urban model. The GBA includes Hong Kong (HK), Macau (MC), and the Pearl River Delta Economic Zone (PRD EZ), which includes nine cities; i.e., Guangzhou (GZ), Shenzhen (SZ), Foshan (FS), Dongguan (DG), Zhuhai (ZH), Zhongshan (ZS), Jiangmen (JM), Huizhou (HZ), and Zhaoqing (ZQ). The WRF domains are larger than the CMAQ domain by at least 3–5 grids to remove the boundary effects of the WRF model on the CMAQ model. The boundary conditions of the outermost D1 domain were obtained from a global chemical transport model GEOS-chem (Lam and Fu, 2010); boundary conditions for the remaining nested domains D2–D4 were obtained from the respective mother domains. Outputs from the SMOKE and CMAQ models were used to drive the ADMS-Urban model.

ADMS-Urban is a street-scale resolution, quasi-Gaussian plume dispersion model from the ADMS family, which has been widely applied worldwide to assess environmental impacts, mitigation strategies, and pollution concentration forecasts (Biggart et al., 2020; Carruthers et al., 1994; Hood et al., 2018; Lao and Teixidó, 2011). The model simulates the dispersion of pollutant emissions in urban areas by representing sources at high spatial resolution (primarily traffic and industry); modeling the influence of urban morphology on dispersion processes (street canyons, building density, tunnels, and road elevation); and applying simplified near-field chemical schemes. Sharp concentration gradients resulting from emissions released from sources such as traffic can be resolved in the model calculations and captured for output using the irregularly spaced receptor grid generated by the model. Spatially variable meteorological parameters from the Weather Research and Forecast (WRF) model, such as wind and surface sensible heat flux, have been used as inputs for the ADMS-Urban model to drive pollutant dispersion. “Background” pollutant concentrations, representing long-range pollutant transport, have been derived from the CMAQ model hourly simulation data. Owing to a lack of representative source parameters (stack heights, efflux parameters), industrial and power plant sources were coarsely represented in the regional model using appropriate factors to disaggregate emissions vertically, whereas an explicit road network was applied to distribute the ground-level traffic emissions in the ADMS-Urban model. Two sets of explicit traffic emissions were prepared: one set emulated the CMAQ grid concentrations that were distributed evenly across the traffic emissions model grid and extracted from the CMAQ model grids; the second set redistributed the CMAQ grid traffic emissions into explicit high-resolution traffic emissions within the facilitated road network. The emulated ADMS-Urban concentrations using the evenly distributed grid emissions were reduced from the ultimate ADMS-Urban concentration calculations to avoid double-counting of emissions. The allocation formula for redistributing the traffic emissions is detailed in Biggart et al. (2020). The road length was determined and calculated on the basis of the CMAQ grids. Different weighting factors were given to different types of roads, but the same factors were assigned to different air pollutants. The road network data were obtained from the OpenStreetMap source (http://openstreetmap.org/), with some minor roads removed to reduce the computational costs. Urban morphology data, such as street canyon and building data, are lacking in the Guangzhou region; these could be considered in the coupled model in future if such data become available. Detailed descriptions of the methodology of coupling a regional model with ADMS-Urban are provided in previous publications (Hood et al., 2018; Stocker et al. 2012).

2.2 Sensitivity scenario design

The control measures affecting emissions from the traffic and industrial sectors were applied in the regional CMAQ model over the PRD EZ, and explicit traffic emissions scenarios were applied to the road traffic network modeled in ADMS-Urban for the Guangzhou urban area. The provincial government in mainland China focuses largely on how the concentrations of air pollutants change if control measures are implemented in the PRD EZ; therefore, we assumed that there were no changes in emissions for HK and MC. The aim of the scenario was to investigate the concentration responses of local control measures. Four potential sensitivity scenarios were designed. As shown in Table 1, the Base case was a business as usual (BAU) scenario for both the regional CMAQ and local ADMS-Urban models. Evaluation of the system was performed for a historical period with readily available measurement data. Meteorological conditions influence the likelihood of O_3 episodes. As higher concentrations were recorded in the spring and autumn of 2019, O_3 episodes in April and May 2019 were chosen for the control measures scenario. Table 1 lists three control scenarios. As NO_x and VOC are important precursors for O_3 formation, the non-linear relationship between the precursors and O_3 is of great importance. Because of the short lifetime of NO_x, which is emitted mainly from the traffic sector, the half traffic case considers a 50% reduction in traffic emissions for all standard pollutants in the coupled modeling system. As the majority of anthropogenic VOC emissions come from the industrial sector, the half industrial VOC case considers a 50% reduction in industrial VOC emissions only in the regional model, with BAU in the local model. The Both control case integrates the control measures in both the half traffic and half industrial VOC scenarios.

2.3 Scenario emissions comparison

It is important to place the "50% reduction" control measures in the context of total emissions. The main reason for halving the precursor emissions was to assess the sensitivity of the air pollutant concentrations to corresponding changes in emission. The brute-force method used in the sensitivity analysis would cause accuracy issues if small emission changes were applied (Clappier et al., 2017; Yarwood et al., 2017). A previous study (Tsimpidi et al., 2008) utilized the same strategy to assess fine particulate matter changes corresponding to halved NO_x and VOC emissions in the United States. However, although $PM_{2.5}$ concentrations were investigated in different regions, no analyses were conducted for specific sectors. Therefore, halving the precursor emissions in sensitivity analyses of air quality modeling is a typical and effective way to evaluate the sectoral concentration responses. A summary of the total annual anthropogenic NO_x, VOC, and $PM_{2.5}$ emissions for the regional model domain covering the central GBA is presented in Figure S3. Both the "point" and "area" emissions categories are considered to represent primarily industrial activities, with VOC emissions affected by the "half industrial VOC" control. Relative to total emissions, the maximum reduction in NO_x is ~17%, and that for $PM_{2.5}$ is only 5%. For VOCs, which are impacted by both control measures in traffic and industrial sectors, emissions are reduced by a much larger amount, 47%. Although the proportions of biogenic and anthropogenic VOC may vary in different seasons and environmental conditions (e.g., temperature, humidity), a previous study estimated that biogenic emissions represent nearly 50% of China's total VOC emissions (Cao et al., 2018). Therefore, biogenic emissions are likely to contribute substantially to VOC emissions in the GBA. As a result, the maximum VOC reduction due to control measures is likely to be closer to 25%. In terms of a reduction in traffic emissions, the modeled scenario corresponds to a reduction in vehicle numbers and/or driving distances, rather than to improvements in vehicle technologies. Although technological improvements (including the introduction of electric vehicles) may reduce vehicle exhaust emissions to zero, non-exhaust particulate emissions, such as brake and tire wear, are a direct result of vehicle activity. Consequently, non-exhaust vehicle emissions are not mitigated by improvements to engine technology, although there may be associated technological improvements in relation to non-exhaust emissions, such as regenerative braking. Daily column emissions comparisons for NO_x, VOC, and $PM_{2.5}$ are provided in the supporting information (Figures S3–S9). We assumed no emissions control activities in HK, as this study focuses on evaluating how air pollution in the PRD EZ changes in response to local controls.

3 Results

The regional model was configured and run for April 1–May 31, 2019. The ADMS-Urban model results were generated for the same period for the urban sub-domains developed as a demonstration area for this study; i.e., a 6-km × 6-km area in central Guangzhou. Period-averaged concentrations were calculated. Both urban and rural locations were selected to illustrate variations in pollution. The period-averaged prediction is the hourly average value for the entire modeling period (April 1–May 31, 2019). This period was chosen owing to the occurrence of frequent O_3 episodes, and the local government is particularly interested in exploring the mechanisms of occurrence in the Guangzhou urban area. A 1-week spin-up period was used.

Statistical parameter performances (Table 2) and time series plots for typical monitoring stations (Figures S10–S12) in the GBA were analyzed to validate the base case of the regional CMAQ model at a 1-km resolution. Table 2 clearly shows that the CMAQ model obtains an acceptable level of accuracy for $PM_{2.5}$ simulations (with mean fractional bias ≤ ±0.6 and mean fractional error ≤ 0.75) according to the criteria proposed by Hu et al. (2016). The averaged O_3 observation is 28.6 ppb, and the mean O_3 simulation is 28.9 ppb, with an Index of Agreement (IOA) of 0.63. Although the CMAQ model underestimates NO_2 concentrations by 2.5 ppb, the IOA of NO_2 is up to 0.57, and the root mean square error is around 10. Overall, the CMAQ model simulation is considered an acceptable input to drive the ADMS-Urban model. In addition to the capability of the CMAQ model to capture the main trend in the time series plots during the modeling period, Figures S13–S15 show the time series comparisons of the base case for both the CMAQ and ADMS-Urban models. Substantial improvement was observed during specific pollution episodes, which illustrates the advantages of coupled urban dispersion models.

3.1 Regional model period-averaged air quality maps

The regional CMAQ model was run for 2 typical months for the base case and the three sensitivity scenarios to drive the respective ADMS-Urban base case and corresponding sensitivity scenarios. The spatial concentration maps of the differences among the scenarios show the concentration changes due to the designed halved emissions in different sectors. Figure 1 shows the simulated spatial concentration maps of period-averaged NO_2 concentrations from the regional CMAQ model, in which the half traffic case dominants by a substantial margin. Therefore, the traffic sector-related scenarios are selected to demonstrate. Figure 1a and b display the period-averaged NO_2 concentrations for major PRD EZ cities for the base case and half traffic case, respectively, at a 1-km grid resolution. As expected, there were clear reductions in NO_2 in Guangzhou and Shenzhen, especially for the road network, owing to the implementation of increased controls on emissions from the traffic sector in these two cities; the traffic sector is the dominant source of NO_2. In terms of the spatial distributions illustrated in Figures 1a and b, NO_2 concentrations are markedly higher in HK (south of Shenzhen), in industrial areas towards Guangzhou, and along shipping lanes than in the urban area in the GBA. Figure 1c quantifies the reductions in NO_2 concentrations for the modeling period, which are as large as 5 ppb in central Guangzhou and Shenzhen.

Figure 2 shows the simulated spatial distribution maps of period-average O_3 concentrations from the CMAQ model for major PRD EZ cities in the (a) Half traffic minus Base case; (b) Half industrial VOC minus Base case, (c) Both controls minus Base case; and (d) Wind Rose diagram showing regional wind directions. The Red shading indicates worsening O_3 concentrations, and blue indicates improving conditions. Figure 2a relates to the effectiveness of the half traffic case. Owing to the substantial reduction in NO_x concentrations (Figure 1c), the half traffic scenario leads to significant increases in O_3 concentrations in Guangzhou and Shenzhen, mainly from the traffic sector. A slight increase (>1 ppb) is observed in other areas, aside from upwind rural areas where an improvement (around 1 ppb) is noted. When the half traffic measures are implemented, the NO_x concentrations drop substantially, leading to less NO_x titration. Therefore, worsening O_3 concentrations are observed in urban areas of Guangzhou and in Shenzhen, especially near road networks. This phenomenon suggests a VOC-limited O_3 formation regime in Guangzhou, which is consistent with the results of previous studies (Wang et al., 2019a; Zhang et al., 2020a). Conversely, in the rural areas to the northeast of the domain, i.e., downwind of the highly polluting areas in mainland China (outside the GBA), O_3 concentrations decrease in response to the controls because lower levels of oxidants (the sum of NO_2 and O_3) are present in the atmosphere.

Figure 2b relates to the effectiveness of the half industrial VOC case on O_3 concentrations. We observe that O_3 concentrations are reduced throughout the domain. This verifies the importance of controlling VOC in areas susceptible to VOC-limited O_3 formation, such as Guangzhou and Shenzhen. The main reason for this observation is that the limited VOCs correspond to lower levels of RO_2 radicals, causing excess NO to react with O_3 in the atmosphere, resulting in less O_3 being generated. During this process, NO_2 concentrations drop owing to the decrease in RO_2 radicals but then increase owing to the consumption of O_3 by excess NO, producing more NO_2. Therefore, the change in net NO_2 would be minimal. Figure 2b also shows that O_3 concentrations are transported from upwind areas, highlighting the impact of regional transport on O_3 concentrations.

Figure 2c shows the contributions of the control cases in both the half traffic and industrial VOC cases simultaneously. Although the O_3 concentrations in urban regions still increase owing to NO_x controls, the magnitude of the increase is mitigated. In most locations outside the urban areas, the O_3 concentrations are reduced. It is noteworthy that, in a large area of the domain (upper left locations in Figure 2c), the trend of O_3 concentrations is inverted, changing from an increase in response to traffic controls to decreases in both control cases. This finding highlights the importance of coordinated controls for both traffic and industrial VOC sources. However, the trend in the downwind area (lower left corner of Figure 2c) remains positive, mainly because of the accumulation of transported O_3, which indicates long-range transport of O_3.

Figure 3 shows the simulated spatial distribution maps of period-averaged $PM_{2.5}$ concentrations from the CMAQ model at a 1-km resolution in the: (a) Base case, (b) Half traffic case; and (c) Difference plot: Both controls minus Base case. Although the $PM_{2.5}$ emissions are not dominated by the traffic sector (Figure S3), a considerable reduction in $PM_{2.5}$ concentrations is observed in the urban Guangzhou area and central Shenzhen, highlighting the strengthened traffic control measures implemented in mega-cities. We consider marine sources as being separate from traffic sources, which is why little change is observed along shipping routes in the half traffic case. The half industrial VOC case has a small impact on $PM_{2.5}$, which will be discussed under the ADMS-Urban results (section 3.2). Figure 3c shows that both control scenarios lead to a considerable reduction in $PM_{2.5}$ concentrations across the mitigation domain, with reductions of up to 3 μg/m³ in central Shenzhen and Guangzhou, focused mainly on the road network.

3.2 Street-level urban model variation of air quality maps.

Concentrations within the ADMS-Urban system in the Guangzhou urban region were calculated at a high spatial resolution (<10 m), specifically for traffic emissions. Hourly concentrations were obtained rather than average concentrations over the 2 months, as was done for the regional CMAQ model domain. For some pollutants, the resultant detailed, hourly air quality maps are consistent with the metrics included in Chinese air quality standards (i.e., the 160 μg/m³ standards for O_3 concentrations, which are applicable in urban areas). Figure 4 shows the simulated high-resolution spatial distribution maps for NO_2 (Guangzhou domain) from the ADMS-Urban model in the: (a) Base case; (b) Half traffic case; (c) Half industrial VOC case; and (d) Both control case during an afternoon in May. High concentrations of NO_2 are clearly observed on the road network. The largest hot spot occurs near the inner ring road and Haiyin Bridge, where traffic is heavy during afternoon peak times. NO_x concentrations in the urban-scale model are determined by emissions sources, pollution dispersion, chemical reactions, and background concentrations. NO_x has a short life cycle; therefore, it is derived mainly from local sources. The half traffic case in Figure 4b shows substantial decreases in NO_2 concentrations throughout the urban domain owing to increasing traffic controls implemented in Guangzhou. The area with excessive NO_2 is significantly reduced. However, local NO_2 concentrations do not change with variations in the reduced industrial VOC cases (Figures 4c). This is mainly because the ADMS-Urban model does not include explicitly industrial emissions, and less NO_2 may be transported from the background regional CMAQ model. Therefore, the case with both controls (Figure 4d) is consistent with the reduced traffic case (Figure 4b).

Figure 5 presents the simulated high-resolution spatial distribution maps of O_3 (Guangzhou domain) from the ADMS-Urban model in the middle of the day during May for: (a) Base case; (b) Half traffic case; (c) Half industrial VOC case; (d) Both control case. For the road network, O_3 concentrations are lower than NO_2 concentrations. As indicated earlier in relation to the regional model results, reducing traffic emissions increases the spatial extent of excessive O_3 in urban areas owing to reduced NO_x titration of O_3 (Figure 5a vs. 5b). Conversely, reducing industrial VOCs leads to a reduction in the area of O_3 exceedance within the local domain (Figure 5a vs. 5c). When both controls are applied in the local area (Figure 5a vs. 5d), the net effect is a slight increase in near-road O_3 concentrations but a decrease in concentrations elsewhere. This is an interesting result that again demonstrates the importance of accounting for both regional and local dispersion and chemistry.

The modeled $PM_{2.5}$ concentrations reflect a different time of day, as the atmospheric conditions associated with $PM_{2.5}$ pollution episodes differ from those associated with O_3 and NO_2. $PM_{2.5}$ concentrations at 18:00 on April 17, 2019 are shown for all four scenarios in Figure 6. Although there is a very small relative reduction in $PM_{2.5}$ emissions (Figure S3), the impact in urban areas is significant during this episode (Figures 6a vs. 6b), as this reduction relates to near-ground traffic sources. The change in industrial VOC emissions has little effect (Figure 6a and 6c) on $PM_{2.5}$ concentrations. In our scenario, the negative impacts on $PM_{2.5}$ on reduced industrial VOC emissions is mainly observed in the background regional CMAQ model, as the ADMS-Urban model has no explicit industrial sources in the reduced industrial VOC scenario. Reducing industrial VOC emissions will directly impact oxidant levels, thus impacting the formation of nitrate, sulfate, and secondary organic aerosols, which are important components of $PM_{2.5}$. When VOC emissions are reduced by 50%, the level of oxidants in summer will increase, leading to increased sulfate or nitrate formation. However, organic matter will be reduced, as more secondary organic aerosol will be generated by increased VOC emissions. Therefore, the net change in $PM_{2.5}$ would be small. This result is consistent with a previous study (Tsimpidi et al., 2008) indicating that controlling industrial VOC emissions may not be an efficient method of controlling $PM_{2.5}$. The simultaneous control of $PM_{2.5}$ and O_3 is a complex issue, and mitigation strategies will vary between areas with different formation regimes (i.e., VOC-limited, NOx limited, or NH_3-rich/poor) (Xing et al., 2019). NH_3 emissions need to be considered to further mitigate $PM_{2.5}$ concentrations in the PRD EZ, as NH_3 has also been detected in eastern China, as well (Geng et al. 2019).

3.3 Modeled concentrations at selected urban and rural locations

This section discusses pointwise concentrations. Where possible, the locations considered relate to air quality measurement sites within the domain. Figure S2 shows the locations of the three reference monitors located within the coupled-system urban model domain of Guangzhou; in addition to other pollutants, NO_2, O_3, and $PM_{2.5}$ concentrations were recorded at these sites. Figure 7 compares the modeled concentrations to the measurements recorded at these three locations, for the base case and three coupled model scenarios in addition to the base case regional model. Box plots of the short-term pollutant metrics are shown, including the daily maximum hourly NO_2, daily maximum 8-hour rolling O_3, and daily mean $PM_{2.5}$. As this is the first time the regional model concentrations have been presented alongside the coupled model concentrations, it is worth noting the differences in the concentrations obtained using the two modeling approaches. Specifically, for NO_2 and

$PM_{2.5}$ at most of the sites, the coupled system predicts higher concentrations than the relatively coarse resolution regional model; for O_3, the coupled system predicts lower concentrations. These differences are expected at the monitoring locations, which are strongly influenced by local road traffic source increments. The respective concentration changes at the selected monitoring stations in the various sensitivity scenarios are similar to the trend illustrated in the comparisons of the spatial concentration map. Figure 7a shows that the NO_2 concentrations are derived mainly from the traffic sector. The effects of NOx titration on the O_3 concentration in Figure 7b drive up the O_3 concentrations; therefore, reducing industrial VOC emissions sources is more effective for O_3 control, revealing a VOC-limited regime in this region.

In terms of the differences in modeled concentrations for the three scenarios, across all sites, the maximum decrease in the median NO_2 hourly metric owing to emissions controls is >11 μg/m³ at the roadside site, which corresponds to the implementation of traffic controls. In terms of O_3, the maximum increase in the median value is >10 μg/m³ for the half traffic scenario. However, this increase is reduced to <7 μg/m³ when both controls are applied simultaneously. The decreases in the median $PM_{2.5}$ is <2 μg/m³ for the low traffic scenario.

It is of interest to quantify the decrease in O_3 concentrations to the northeast of the model domain, as shown in Figures 2c. Unfortunately, data were unavailable for this rural location. Furthermore, the coupled system has only been configured for the example urban sub-domains in Guangzhou. Consequently, the only comparison to be made at this location is between concentrations calculated by the regional model. Concentration data for the location indicated by the white star in Figure 2 are presented in Figure 8; the metrics calculated for NO_2, O_3, and $PM_{2.5}$ are the same as those presented in Figure 7. Of the three pollutants modeled at this rural location, the different emissions mitigation options only significantly alter the NO_2 concentrations. This is unsurprising because Figure S3 shows that traffic emissions contribute a large proportion of the NO_x emissions over the whole domain, so changes to NO_x emissions are likely to impact NO_2 concentrations in either rural or urban areas. Conversely, traffic makes up a relatively small proportion of primary $PM_{2.5}$ emissions in rural areas, where ambient $PM_{2.5}$ levels are more influenced by industrial point and area source emissions, in addition to the formation of secondary organic and inorganic particulate matter (Wu and Xie, 2018).

In terms of O_3, there is a relatively minimal reduction in terms of the median maximum 8-hour averaged concentrations resulting from the reduced VOC emissions scenario. This is perhaps surprising when considering Figure 5 as, for the corresponding scenarios, decreases of tens of μg/m³ are shown throughout the urban model domain. To understand this, it is helpful to look at a time series of modeled O_3 concentrations during an episode (Figure 9a). Here, we see that although there usually is very little difference in concentrations, the mitigation scenarios have a substantial impact in this rural location when O_3 levels are at their highest (up to 15 μg/m³ for the 8-hour rolling average metric) and with greater hourly concentration differences (up to 25 μg/m³) over the same period.

4 Discussion

A regional-to-local scale coupled modeling system consisting of a regional CMAQ model (Zhang et al., 2020) and a street-scale ADMS-Urban model (Biggart et al., 2020) was implemented to explore the sensitivity of NO_2, O_3, and $PM_{2.5}$ to controls on traffic sources and industrial VOC emissions in the GBA, at varied resolutions. The high-resolution concentration gradients (<10 m) have been cautiously resolved (Figures 4, 5, and 6) using specific traffic emissions, which aid the assessment of health impacts in densely populated urban regions (Schmitz et al., 2019). A growing number of studies using satellite instruments, land use regression models, or directly measured personal exposure have been conducted to obtain high-resolution spatial air pollution concentration maps (Apte et al., 2017), highlighting the importance of high-resolution (10–20 m) spatial datasets. Our coupled modeling system makes uses of a coarse regional model that provides time-varying background concentrations to drive street-level air dispersion models such as ADMS-Urban, which specializes in capturing rapid chemical reactions. The initial results of the presented Guangzhou case are promising, providing more information on NO_x–O_3 sensitivity that is consistent with findings from previous modeling studies (Chen et al., 2021; Ma et al., 2021; Wu et al., 2021; Zhang et al., 2021a,). This finding indicates that synergistic controls of NO_x and VOCs are promising means for the simultaneous mitigation of $PM_{2.5}$ and O_3, consistent with the findings of Wu et al. (2021). By coupling the regional-to-local scale model, the background concentration fields play a key role in the spatial variations of urban modeling simulations (Figures 4c, 5c, and 6c). Further efforts to refine emissions in both the regional and urban-scale models are necessary, especially for more explicit emissions sectors.

More stringent controls on industrial VOC emissions are found to be essential for inverting O_3 concentrations from a worsening trend to a slight improvement (Figures 2b and 4b). This finding sheds light on the importance of applying stringent VOC control measures to the industrial sector in the near future. Previous studies (Chen et al., 2019; Mozaffar et al., 2020) have shown the efficiency of O_3 controls in response to different VOC/NO_x ratios and varying O_3 formation regimes. The effects of reducing these ratios should be further explored from a high-resolution perspective in light of the substantial influence of biogenic VOC emissions on climate change (Li et al., 2018).

Urban/rural locations were selected for analysis of the relative changes in the metric of different pollutants during pollution episodes. The magnitude of these relative changes should be taken in the context of the metric considered: hourly values (i.e., NO_2) demonstrate the greatest variations because the maximum differences at peak traffic times are quantified; conversely, for daily averaged values (i.e., for $PM_{2.5}$), the impact of peak values is smoothed out by the inclusion of hours where pollutant concentrations may be dominated by regional rather than local air pollution. O_3 episodes are currently of particular interest to government officials and stakeholders. Our modeling work has demonstrated while O_3 concentrations increase in urban areas as a result of the mitigation options considered, O_3 concentrations decrease in upwind areas. Inspection of the modeled pollutant concentrations at a rural location to the northeast of the modeling domain during an O_3 episode shows that the concentrations were reduced by up to 15 $\mu g/m^3$ for the 8-hour metric and up to 25 $\mu g/m^3$ for the 1-hour metric.

Although the implemented coupled CMAQ–ADMS-Urban modeling system is capable of resolving the fine concentration gradient near road networks in this study, several limitations remain to be further investigated in future studies. First, more complete emission sectors, such as point, industry, or residential sources, should be included to construct holistic, high-resolution concentration maps. Second, the urban domain should be further expanded to cover the whole GBA to obtain more complete measurements for model validation and exploration of photochemical mechanisms. Finally, the street canyon module and more detailed building data will most certainly benefit accurate calculations of the dispersion of air pollutants.

5 Conclusion

To address the challenges of controlling $PM_{2.5}$ and O_3 concentrations simultaneously using an ultrahigh spatial resolution approach, this study presents the regional air quality CMAQ model coupled to the street-scale ADMS-Urban model. This coupled system allows a thorough assessment of the impacts of halved traffic emissions and industrial VOC emissions on ambient NO_2, O_3, and $PM_{2.5}$ concentrations, creating a holistic representation of pollution mitigation at a range of spatial resolutions and highlighting the interactions between emissions, meteorological conditions, and O_3 concentrations. Both the regional and urban-scale models illustrate the VOC-limited O_3 formation regime in Guangzhou and highlight the importance of synergistic control of NOx and VOC for mitigating O_3 and $PM_{2.5}$ pollutions, especially with regard to strengthening controls on industrial VOC sources. With coupling, the street-scale ADMS-Urban model resolves the sharp concentration gradients in the vicinity of road sources. Urban and rural locations in central Guangzhou are used as examples to better interpret the findings, which will be beneficial for government policymaking.

Although the detailed mitigation pathways modeled here support the second phase of the Air Pollution Prevention and Control Action Plan—the Three-Year Action Plan for Clean Air—released by the State Council of China in 2018, further refinements will be required through future studies. Subsequent studies will benefit from analysis using a more comprehensive observational pollutant concentrations dataset; application of the model over larger urban areas in the region; and application of the coupled street-scale air quality modeling system to similar urban cities. In addition, a more advanced emission preparation methodology (Lam et al., 2021) could be applied to minimize the uncertainties associated with the emission inventory, and more elaborate emission sources could be modeled explicitly in the ADMS-Urban model; e.g., industrial stacks (Hood et al., 2018). As meteorological factors (e.g., wind) are of great importance to coupled model simulations (Wang et al., 2019b), improving the representation of urban morphological data in the model could improve baseline model biases. Finally, assessing reduction in the NO_x/VOC radio in various areas of a city or in different cities should be cautiously assessed for efficient complex co-photochemical controls.

Acknowledgements

We sincerely thank the Hong Kong Environmental Protection Department (EPD) for providing the bottom-up emission inventory. We appreciate the Guangdong Environmental Monitoring Centre, Macao EPD, and HK EPD for offering observational data to validate the model runs. The authors would like to acknowledge funding from the Newton Fund through Innovate UK as part of the project entitled Air Pollution Monitoring and Very High Resolution Early Warning Platform for Guangdong (project number 104313), Science and Technology Planning Project of Guangdong Province (2018A050501004), HSBC 150th

Anniversary Charity Programme through the PRAISE-HK project, and the Research Grants Council of the Hong Kong Government (Project No. T24/504/17). We sincerely appreciate the editors and anonymous reviewers for their constructive suggestions and thoughtful comments.

Data Availability Statement

The emission inventory data can be accessed from the Hong Kong EPD website (https://www.epd.gov.hk/epd/english/environmentinhk/air/data/emission_inve.html). The observational data can be accessed from China National Environmental Monitoring Centre website (http://www.cnemc.cn) and the Hong Kong EPD website (https://www.epd.gov.hk/epd/english/environmentinhk/air/data/air_data.html). The OpenStreetMap source is available at http://openstreetmap.org/. The Multi-resolution Emission (MEIC) data can refer to the released data set from Tsinghua University (Tong et al., 2020).

References

Apte, J.S., Messier, K.P., Gani, S., Brauer, M., Kirchstetter, T.W., Lunden, M.M., Marshall, J.D., Portier, C.J., Vermeulen, R.C. and Hamburg, S.P., 2017. High-resolution air pollution mapping with Google street view cars: exploiting big data. Environmental Science and Technology, 51(12), pp.6999-7008.

Biggart, M., Stocker, J., Doherty, R.M., Wild, O., Hollaway, M., Carruthers, D., Li, J., Zhang, Q., Wu, R., Kotthaus, S., 2020. Street-scale air quality modelling for Beijing during a winter 2016 measurement campaign. Atmospheric Chemistry and Physics 20, 2755-2780.

Cai, S., Ma, Q., Wang, S., Zhao, B., Brauer, M., Cohen, A., Martin, R.V., Zhang, Q., Li, Q., Wang, Y., 2018. Impact of air pollution control policies on future $PM_{2.5}$ concentrations and their source contributions in China. Journal of Environmental Management 227, 124-133.

Cao, H., Fu, T.M., Zhang, L., Henze, D.K., Miller, C.C., Lerot, C., Abad, G.G., Smedt, I.D., Zhang, Q., Roozendael, M.V. and Hendrick, F., 2018. Adjoint inversion of Chinese non-methane volatile organic compound emissions using space-based observations of formaldehyde and glyoxal. Atmospheric Chemistry and Physics, 18(20), pp.15017-15046.

Carruthers, D., Holroyd, R., Hunt, J., Weng, W., Robins, A., Apsley, D., Thompson, D., Smith, F., 1994. UK-ADMS: A new approach to modelling dispersion in the earth's atmospheric boundary layer. Journal of Wind Engineering and Industrial Aerodynamics 52, 139-153.

Clappier, A., Belis, C. A., Pernigotti, D., & Thunis, P. 2017. Source apportionment and sensitivity analysis: two methodologies with two different purposes. Geoscientific Model Development, *10*(11), 4245-4256.

Che, W., Frey, H.C., Fung, J.C., Ning, Z., Qu, H., Lo, H.K., Chen, L., Wong, T.-W., Wong, M.K., Lee, O.C., 2020. PRAISE-HK: A personalized real-time air quality informatics system for citizen participation in exposure and health risk management. Sustainable Cities and Society 54, 101986.

Chen, X., Situ, S., Zhang, Q., Wang, X., Sha, C., Zhouc, L., Wu, L., Wu, L., Ye, L. and Li, C., 2019. The synergetic control of NO2 and O3 concentrations in a manufacturing city of southern China. Atmospheric Environment, 201, pp.402-416.

Cheng, J., Tong, D., Zhang, Q., Liu, Y., Lei, Y., Yan, G., Yan, L., Yu, S., Cui, R.Y., Clarke, L., 2021. Pathways of China's $PM_{2.5}$ air quality 2015–2060 in the context of carbon neutrality. National Science Review. 0, nwab078.

Conibear, L., Reddington, C.L., Silver, B.J., Knote, C., Arnold, S.R., Spracklen, D.V., 2021. Regional policies targeting residential solid fuel and agricultural emissions can improve air quality and public health in the Greater Bay Area and across China. GeoHealth, e2020GH000341.

Cui, R.Y., Hultman, N., Cui, D., McJeon, H., Yu, S., Edwards, M.R., Sen, A., Song, K., Bowman, C., Clarke, L., 2021. A plant-by-plant strategy for high-ambition coal power phaseout in China. Nature Communications 12, 1-10.

Geng, G., Xiao, Q., Zheng, Y., Tong, D., Zhang, Y., Zhang, X., ... & Liu, Y. 2019. Impact of China's air pollution prevention and control action plan on PM 2.5 chemical composition over eastern China. Science China Earth Sciences, *62*(12), 1872-1884.

Gong, K., Li, L., Li, J., Qin, M., Wang, X., Ying, Q., Liao, H., Guo, S., Hu, M., Zhang, Y., 2021. Quantifying the impacts of inter-city transport on air quality in the Yangtze River Delta urban agglomeration, China:

Implications for regional cooperative controls of $PM_{2.5}$ and O_3. Science of the Total Environment 779, 146619.

Hood, C., MacKenzie, I., Stocker, J., Johnson, K., Carruthers, D., Vieno, M., Doherty, R., 2018. Air quality simulations for London using a coupled regional-to-local modelling system. Atmospheric Chemistry and Physics 18, 11221-11245.

Hood, C., Stocker, J., Seaton, M., Johnson, K., O'Neill, J., Thorne, L., Carruthers, D., 2021. Comprehensive evaluation of an advanced street canyon air pollution model. Journal of the Air & Waste Management Association 71, 247-267.

Hu, J., Chen, J., Ying, Q. and Zhang, H., 2016. One-year simulation of ozone and particulate matter in China using WRF/CMAQ modeling system. Atmospheric Chemistry and Physics, 16(16), pp.10333-10350.

Jiang, X., Hong, C., Zheng, Y., Zheng, B., Guan, D., Gouldson, A., Zhang, Q., He, K., 2015. To what extent can China's near-term air pollution control policy protect air quality and human health? A case study of the Pearl River Delta region. Environmental Research Letters 10, 104006.

Jiang, X., Yoo, E.-h., 2018. The importance of spatial resolutions of community multiscale air quality (CMAQ) models on health impact assessment. Science of the Total Environment 627, 1528-1543.

Lam, Y., Fu, J., 2010. A novel downscaling technique for the linkage of global and regional air quality modeling. Atmospheric Chemistry and Physics, 4013.

Lam, Y.F., Cheung, C.C., Zhang, X., Fu, J.S., Fung, J.C.H., 2021. Development of New Emission Reallocation Method for Industrial Nonpoint Source in China. Atmospheric Chemistry and Physics, 21, 12895–12908.

Lao, J., Teixidó, O., 2011. Air quality model for Barcelona. Air Pollution 19, 25-36.

Li, K., Jacob, D.J., Liao, H., Shen, L., Zhang, Q., Bates, K.H., 2019a. Anthropogenic drivers of 2013–2017 trends in summer surface ozone in China. Proceedings of the National Academy of Sciences 116, 422-427.

Li, K., Jacob, D.J., Liao, H., Zhu, J., Shah, V., Shen, L., Bates, K.H., Zhang, Q., Zhai, S., 2019b. A two-pollutant strategy for improving ozone and particulate air quality in China. Nature Geoscience 12, 906-910.

Li, L., Hu, J., Li, J., Gong, K., Wang, X., Ying, Q., Qin, M., Liao, H., Guo, S., Hu, M., 2021a. Modelling air quality during the EXPLORE-YRD campaign–Part II. Regional source apportionment of ozone and $PM_{2.5}$. Atmospheric Environment 247, 118063.

Li, M., Zhang, D., Li, C.-T., Selin, N.E., Karplus, V.J., 2019c. Co-benefits of China's climate policy for air quality and human health in China and transboundary regions in 2030. Environmental Research Letters 14, 084006.

Li, N., He, Q., Greenberg, J., Guenther, A., Li, J., Cao, J., Wang, J., Liao, H., Wang, Q., Zhang, Q., 2018. Impacts of biogenic and anthropogenic emissions on summertime ozone formation in the Guanzhong Basin, China. Atmospheric Chemistry and Physics 18, 7489-7507.

Li, Y., Xu, H., Tang, K., Lau, A., Fung, J., Zhang, X., 2021b. An Ensemble Assessment of the Effectiveness of Vehicular Emission Control Programs for Air Quality Improvement in Hong Kong. Atmospheric Environment, 118571.

Liu, T., Wang, C., Wang, Y., Huang, L., Li, J., Xie, F., Zhang, J., Hu, J., 2020. Impacts of model resolution on predictions of air quality and associated health exposure in Nanjing, China. Chemosphere 249, 126515.

Malkin, T.L., Heard, D.E., Hood, C., Stocker, J., Carruthers, D., MacKenzie, I.A., Doherty, R.M., Vieno, M., Lee, J., Kleffmann, J. and Laufs, S., 2016. Assessing chemistry schemes and constraints in air quality models used to predict ozone in London against the detailed Master Chemical Mechanism. Faraday Discussions, 189, pp.589-616.

Ma, Y., Fu, S., Gao, S., Zhang, S., Che, X., Wang, Q. and Jiao, Z., 2021. Update on volatile organic compound (VOC) source profiles and ozone formation potential in synthetic resins industry in China. Environmental Pollution, p.118253.

Mozaffar, A., Zhang, Y.L., Fan, M., Cao, F. and Lin, Y.C., 2020. Characteristics of summertime ambient VOCs and their contributions to O_3 and SOA formation in a suburban area of Nanjing, China. Atmospheric Research, 240, p.104923.

Qin, Y., Wagner, F., Scovronick, N., Peng, W., Yang, J., Zhu, T., Smith, K.R., Mauzerall, D.L., 2017. Air quality, health, and climate implications of China's synthetic natural gas development. Proceedings of the National Academy of Sciences 114, 4887-4892.

Schmitz, O., Beelen, R., Strak, M., Hoek, G., Soenario, I., Brunekreef, B., ... & Karssenberg, D. 2019. High resolution annual average air pollution concentration maps for the Netherlands. Scientific Data, *6*(1), 1-12.

Silveira, C., Ferreira, J., Miranda, A.I., 2019. The challenges of air quality modelling when crossing multiple spatial scales. Air Quality, Atmosphere & Health 12, 1003-1017.

Silver, B., Conibear, L., Reddington, C.L., Knote, C., Arnold, S.R., Spracklen, D.V., 2020. Pollutant emission reductions deliver decreased $PM_{2.5}$-caused mortality across China during 2015–2017. Atmospheric Chemistry and Physics 20, 11683-11695.

Stocker, J., Hood, C., Carruthers, D., McHugh, C., 2012. ADMS-Urban: developments in modelling dispersion from the city scale to the local scale. International Journal of Environment and Pollution 50, 308-316.

Tao, H., Xing, J., Zhou, H., Pleim, J., Ran, L., Chang, X., Wang, S., Chen, F., Zheng, H., Li, J., 2020. Impacts of improved modeling resolution on the simulation of meteorology, air quality, and human exposure to $PM_{2.5}$, O_3 in Beijing, China. Journal of Cleaner Production 243, 118574.

Tong, D., Cheng, J., Liu, Y., Yu, S., Yan, L., Hong, C., Qin, Y., Zhao, H., Zheng, Y., Geng, G., 2020. Dynamic projection of anthropogenic emissions in China: methodology and 2015–2050 emission pathways under a range of socio-economic, climate policy, and pollution control scenarios. Atmospheric Chemistry and Physics 20, 5729-5757.

Tsimpidi, A. P., Karydis, V. A., & Pandis, S. N. (2008). Response of fine particulate matter to emission changes of oxides of nitrogen and anthropogenic volatile organic compounds in the Eastern United States. Journal of the Air & Waste Management Association, 58(11), 1463-1473.

Wang, N., Lyu, X., Deng, X., Huang, X., Jiang, F., Ding, A., 2019a. Aggravating O_3 pollution due to NO_x emission control in eastern China. Science of the Total Environment 677, 732-744.

Wang, P., Guo, H., Hu, J., Kota, S.H., Ying, Q., Zhang, H., 2019b. Responses of $PM_{2.5}$ and O_3 concentrations to changes of meteorology and emissions in China. Science of the Total Environment 662, 297-306.

Wang, X., Li, L., Gong, K., Mao, J., Hu, J., Li, J., Liu, Z., Liao, H., Qiu, W., Yu, Y., 2021. Modelling air quality during the EXPLORE-YRD campaign–Part I. Model performance evaluation and impacts of meteorological inputs and grid resolutions. Atmospheric Environment 246, 118131.

Wu, J., Wang, Y., Liang, J., Yao, F., 2021. Exploring common factors influencing $PM_{2.5}$ and O_3 concentrations in the Pearl River Delta: Tradeoffs and synergies. Environmental Pollution, 117138.

Wu, R., Liu, F., Tong, D., Zheng, Y., Lei, Y., Hong, C., Li, M., Liu, J., Zheng, B., Bo, Y., 2019. Air quality and health benefits of China's emission control policies on coal-fired power plants during 2005–2020. Environmental Research Letters 14, 094016.

Wu, R., Xie, S., 2018. Spatial distribution of secondary organic aerosol formation potential in China derived from speciated anthropogenic volatile organic compound emissions. Environmental Science and Technology 52, 8146-8156.

Xing, J., Ding, D., Wang, S., Dong, Z., Kelly, J. T., Jang, C., ... & Hao, J. (2019). Development and application of observable response indicators for design of an effective ozone and fine-particle pollution control strategy in China. Atmospheric Chemistry and Physics, 19(21), 13627-13646.

Yarwood, G., Morris, R. E., & Wilson, G. M. (2007). Particulate matter source apportionment technology (PSAT) in the CAMx photochemical grid model. In Air Pollution Modeling and Its Application XVII (pp. 478-492). Springer, Boston, MA.

Yli-Pelkonen, V., Scott, A.A., Viippola, V., Setälä, H., 2017. Trees in urban parks and forests reduce O_3, but not NO_2 concentrations in Baltimore, MD, USA. Atmospheric Environment 167, 73-80.

Zhang, C., Chen, M., Li, R., Ding, Y., Lin, H., 2015. A virtual geographic environment system for multiscale air quality analysis and decision making: A case study of SO_2 concentration simulation. Applied Geography 63, 326-336.

Zhang, X., Fung, J.C., Lau, A.K., Hossain, M.S., Louie, P.K., Huang, W., 2021a. Air quality and synergistic health effects of ozone and nitrogen oxides in response to China's integrated air quality control policies during 2015–2019. Chemosphere 268, 129385.

Zhang, X., Fung, J.C., Lau, A.K., Zhang, S., Huang, W., 2021b. Improved Modeling of Spatiotemporal Variations of Fine Particulate Matter Using a Three-Dimensional Variational Data Fusion Method. Journal of Geophysical Research: Atmospheres 126, e2020JD033599.

Zhang, X., Fung, J.C., Zhang, Y., Lau, A.K., Leung, K.K., Huang, W.W., 2020. Assessing $PM_{2.5}$ emissions in 2020: The impacts of integrated emission control policies in China. Environmental Pollution 263, 114575.

Zhao, H., Chen, K., Liu, Z., Zhang, Y., Shao, T., Zhang, H., 2021. Coordinated control of $PM_{2.5}$ and O_3 is urgently needed in China after implementation of the "Air pollution prevention and control action plan". Chemosphere 270, 129441.

Table captions

Table 1. Summary of the Scenarios for Data Assimilation.

Table 2. Statistical performance of the CMAQ base scenario in Domain 4, at a resolution of 1 km. The units of NO_2 and O_3 are ppb, the unit of $PM_{2.5}$ is μg/m^3.

Table 1. Scenario design for the CMAQ–ADMS-Urban coupling system integrating the regional CMAQ model and local street-level ADMS-Urban model.

Scenarios	**I. Base case**	**II. Half Traffic case**	**III. Half Industry VOC case**	**IV. Both Control case**
Scenario description	Business As Usual (BAU)	50% reduction in traffic emissions	50% reduction in industrial VOC emissions	Scenarios II & III
Regional CMAQ model emissions	BAU	50% emission reduction in Mobile sector (all pollutants)	50% emission reduction in VOC from Industrial sector	50% emission reduction in a) mobile sector (all pollutants) and b) VOC emissions from the industrial sector
Local street-level model emissions	BAU	50% reduction in emissions from explicitly defined road traffic sources	BAU	50% reduction in emissions from explicitly defined road traffic sources

Table 2. Statistical performance of the CMAQ base scenario in regional model domain 4, at a resolution of 1 km. The units of NO_2 and O_3 are ppb, the unit of $PM_{2.5}$ is μg/m^3.

	OBS	Model	IOA	RMSE	MNB	MNE	MFB	MFE
NO_2	15.3	12.8	0.57	10.37	0.26	0.81	-0.19	0.61
O_3	28.6	28.9	0.63	18.51	1.32	1.63	0.18	0.61
$PM_{2.5}$	18.2	13.92	0.49	12.03	0.07	0.65	-0.25	0.57

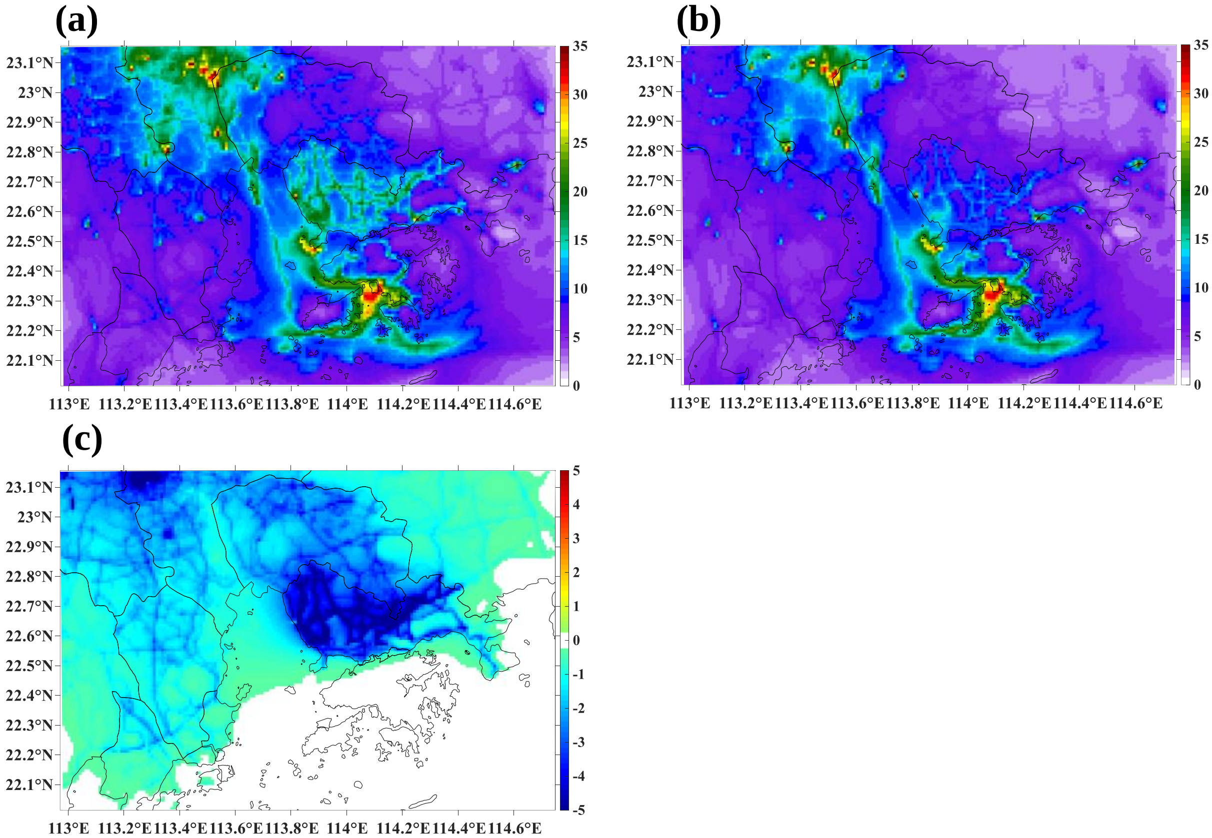
(a)
(b)
(c)
23.1°N
23°N
22.9°N
22.8°N
22.7°N
22.6°N
22.5°N
22.4°N
22.3°N
22.2°N
22.1°N
113°E
113.2°E
113.4°E
113.6°E
113.8°E
114°E
114.2°E
114.4°E
114.6°E
35
30
25
20
15
10
5
0
5
4
3
2
1
0
-1
-2
-3
-4
-5

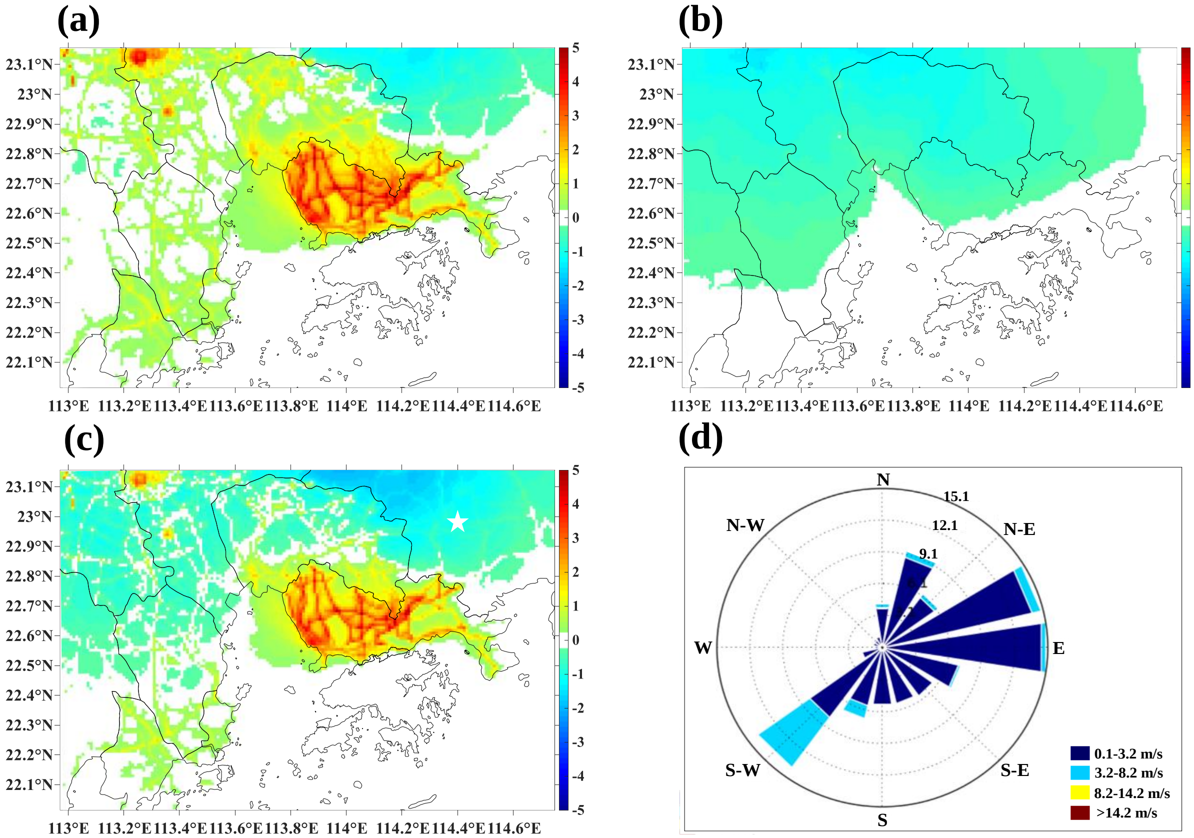
(a)
(b)
(c)
(d)
23.1°N
23°N
22.9°N
22.8°N
22.7°N
22.6°N
22.5°N
22.4°N
22.3°N
22.2°N
22.1°N
113°E
113.2°E
113.4°E
113.6°E
113.8°E
114°E
114.2°E
114.4°E
114.6°E
5
4
3
2
1
0
-1
-2
-3
-4
-5
N
N-E
E
S-E
S
S-W
W
N-W
15.1
12.1
9.1
0.1-3.2 m/s
3.2-8.2 m/s
8.2-14.2 m/s
>14.2 m/s

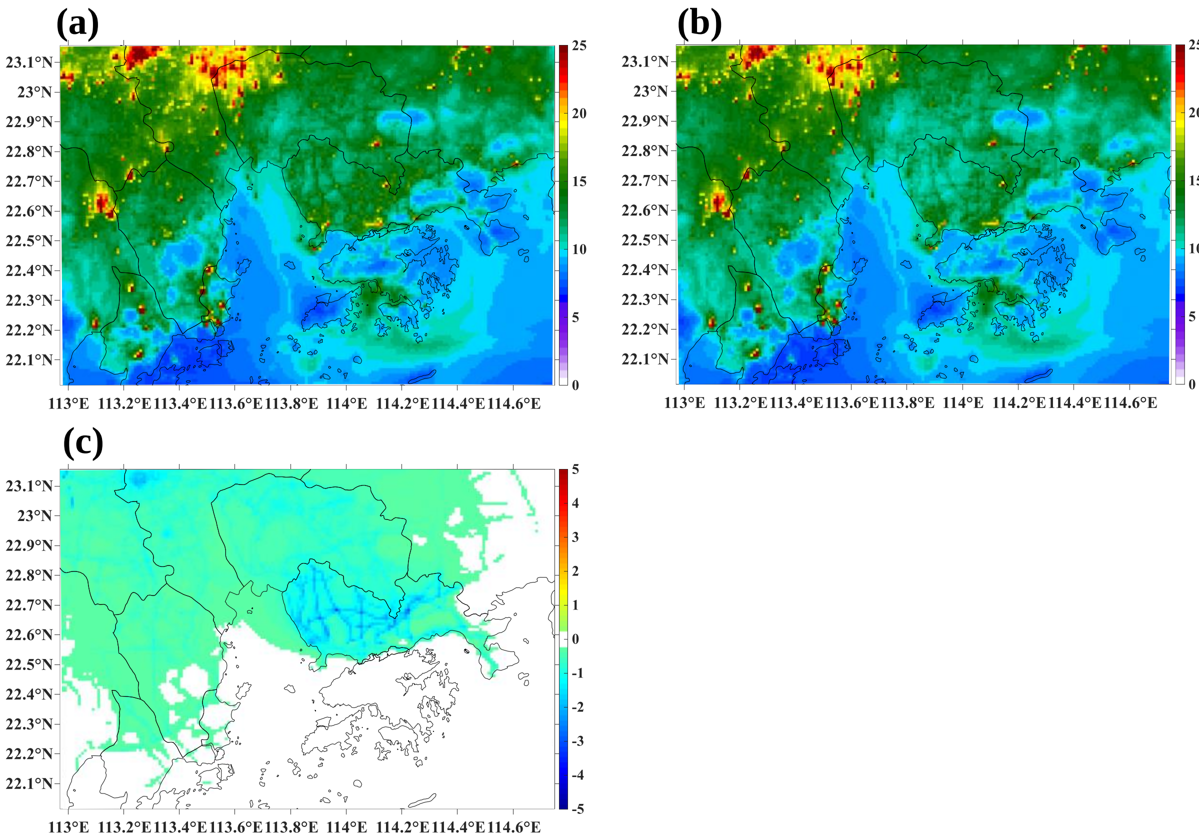
(a)
(b)
(c)
23.1°N
23°N
22.9°N
22.8°N
22.7°N
22.6°N
22.5°N
22.4°N
22.3°N
22.2°N
22.1°N
113°E
113.2°E
113.4°E
113.6°E
113.8°E
114°E
114.2°E
114.4°E
114.6°E
25
20
15
10
5
0
5
4
3
2
1
0
-1
-2
-3
-4
-5

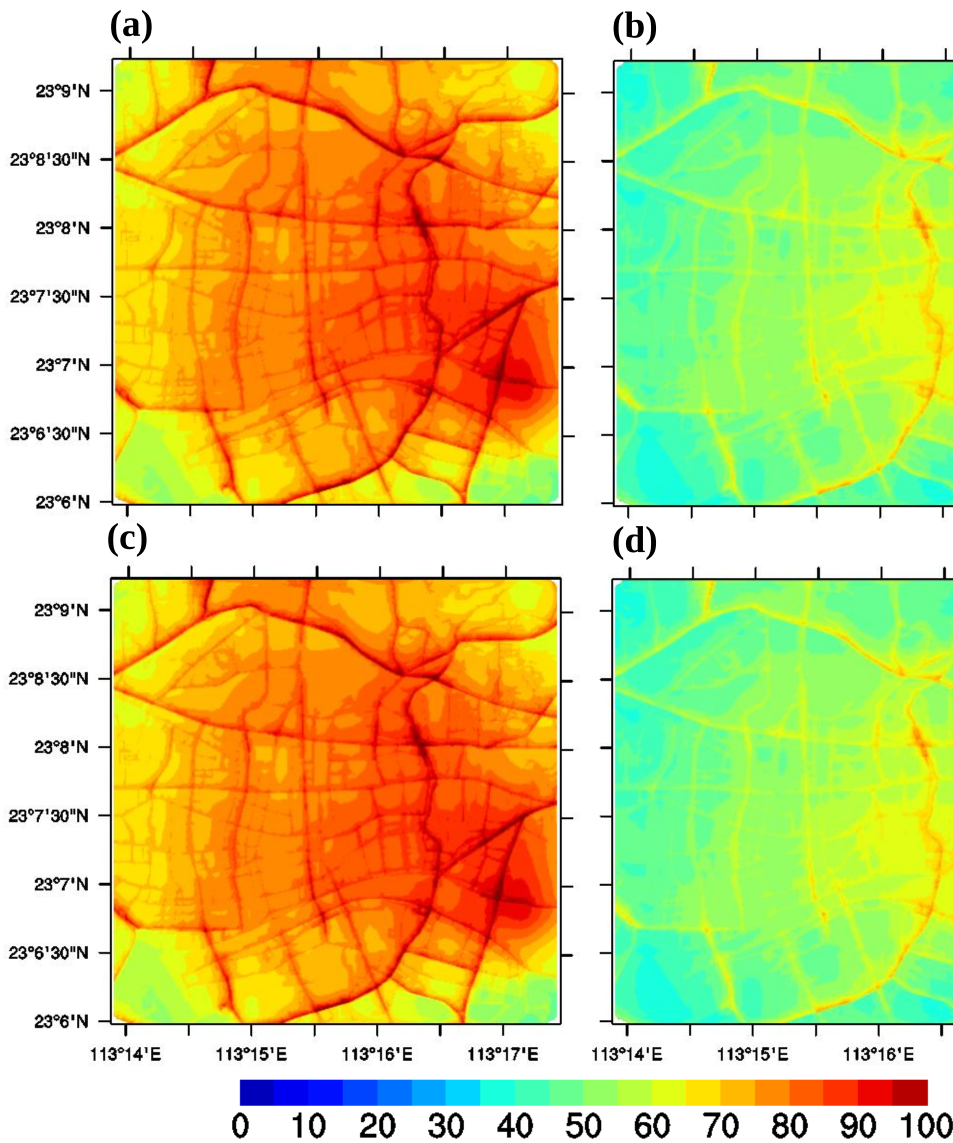

(a)
(b)
(c)
(d)
23°9'N
23°8'30"N
23°8'N
23°7'30"N
23°7'N
23°6'30"N
23°6'N
113°14'E
113°15'E
113°16'E
113°17'E
0 10 20 30 40 50 60 70 80 90 100

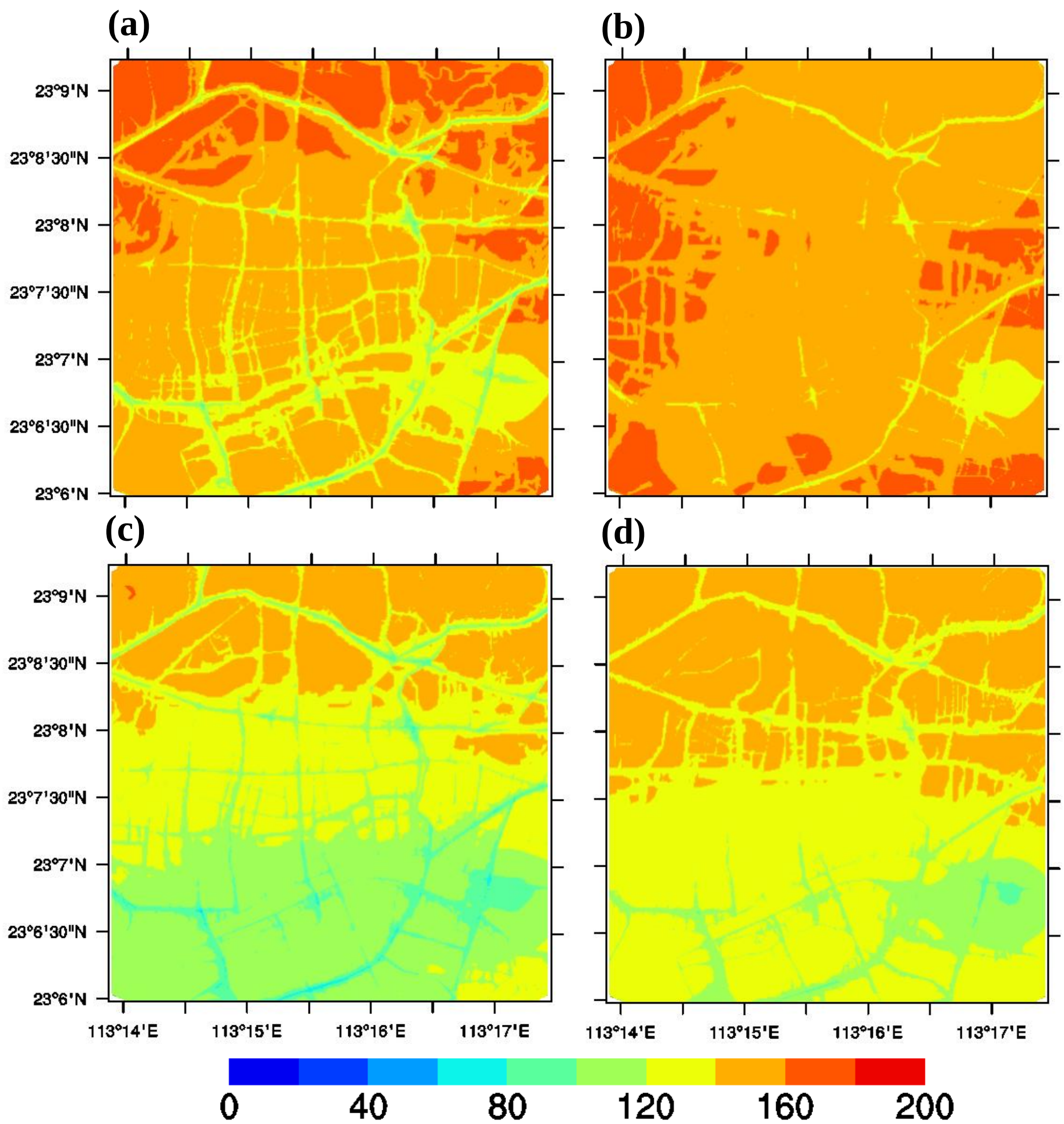

(a)
(b)
(c)
(d)
23°9'N
23°8'30"N
23°8'N
23°7'30"N
23°7'N
23°6'30"N
23°6'N
113°14'E
113°15'E
113°16'E
113°17'E
0
40
80
120
160
200

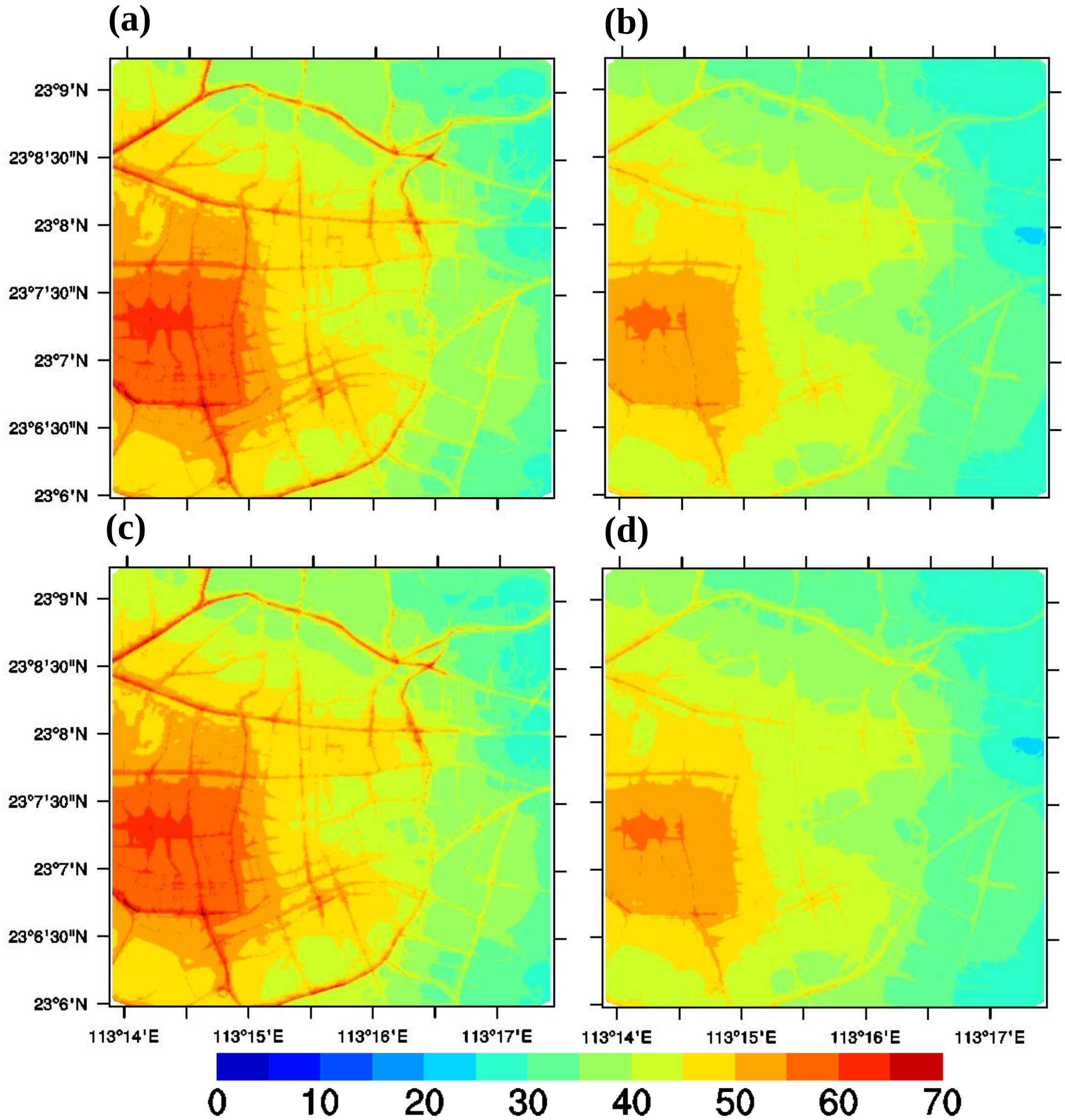

(a)
(b)
(c)
(d)
23°9'N
23°8'30"N
23°8'N
23°7'30"N
23°7'N
23°6'30"N
23°6'N
113°14'E
113°15'E
113°16'E
113°17'E
0
10
20
30
40
50
60
70

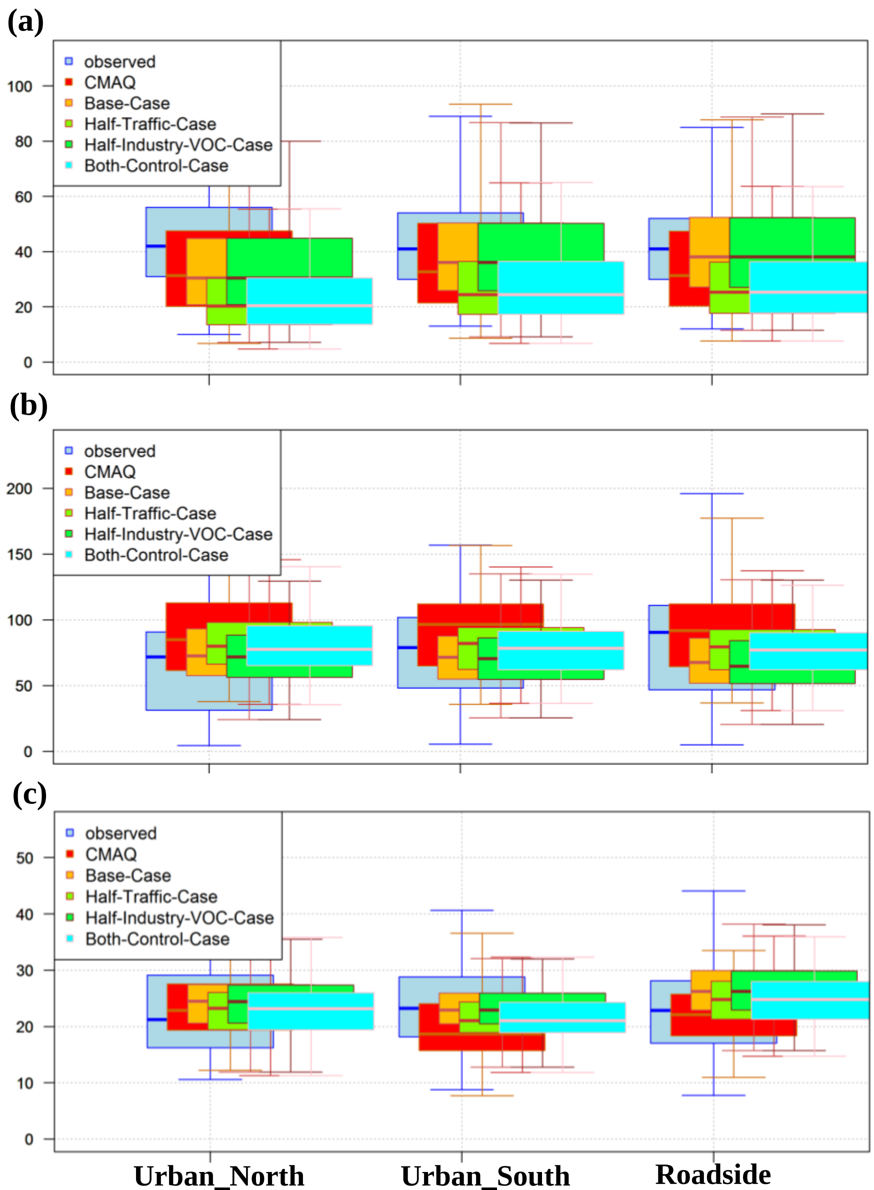

(a)
observed
CMAQ
Base-Case
Half-Traffic-Case
Half-Industry-VOC-Case
Both-Control-Case
0
20
40
60
80
100
(b)
observed
CMAQ
Base-Case
Half-Traffic-Case
Half-Industry-VOC-Case
Both-Control-Case
0
50
100
150
200
(c)
observed
CMAQ
Base-Case
Half-Traffic-Case
Half-Industry-VOC-Case
Both-Control-Case
0
10
20
30
40
50
Urban_North
Urban_South
Roadside

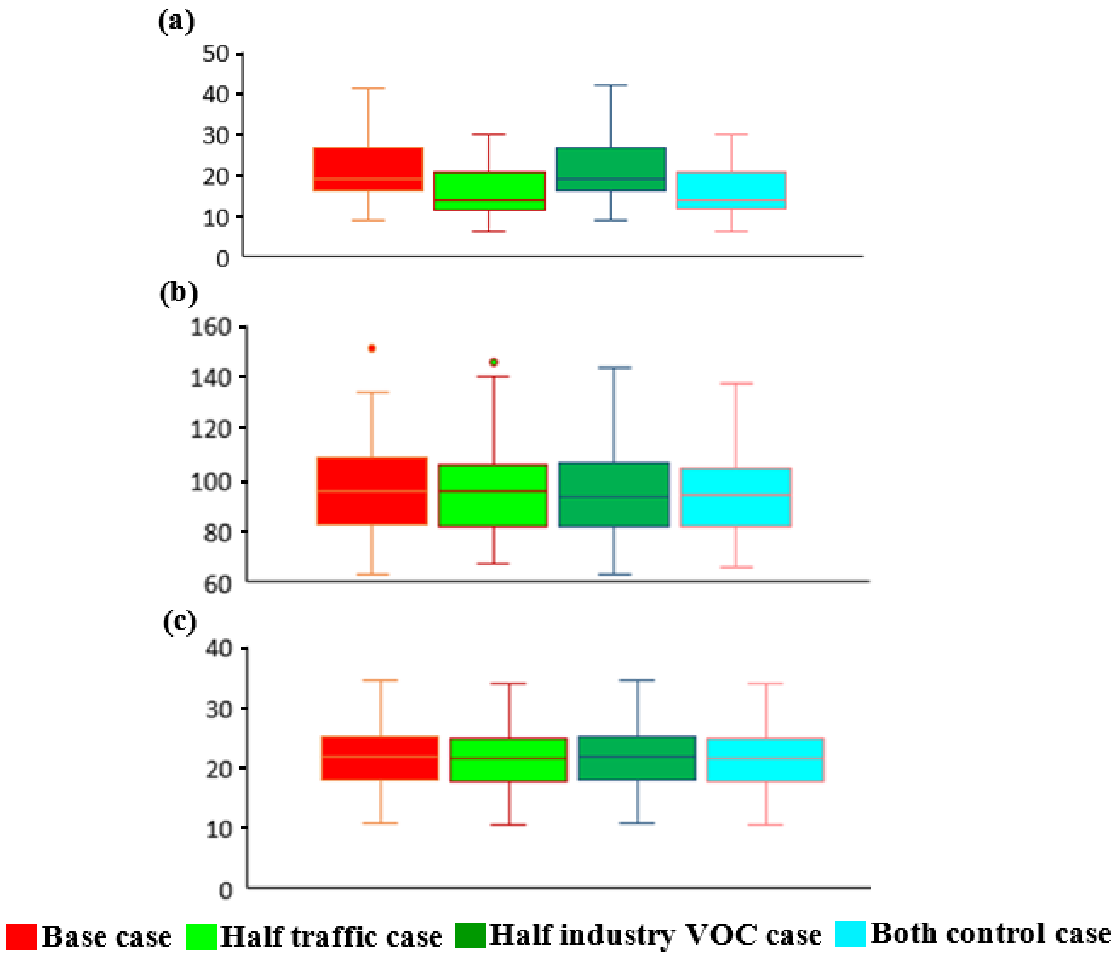

(a)
50
40
30
20
10
0
(b)
160
140
120
100
80
60
(c)
40
30
20
10
0
Base case
Half traffic case
Half industry VOC case
Both control case

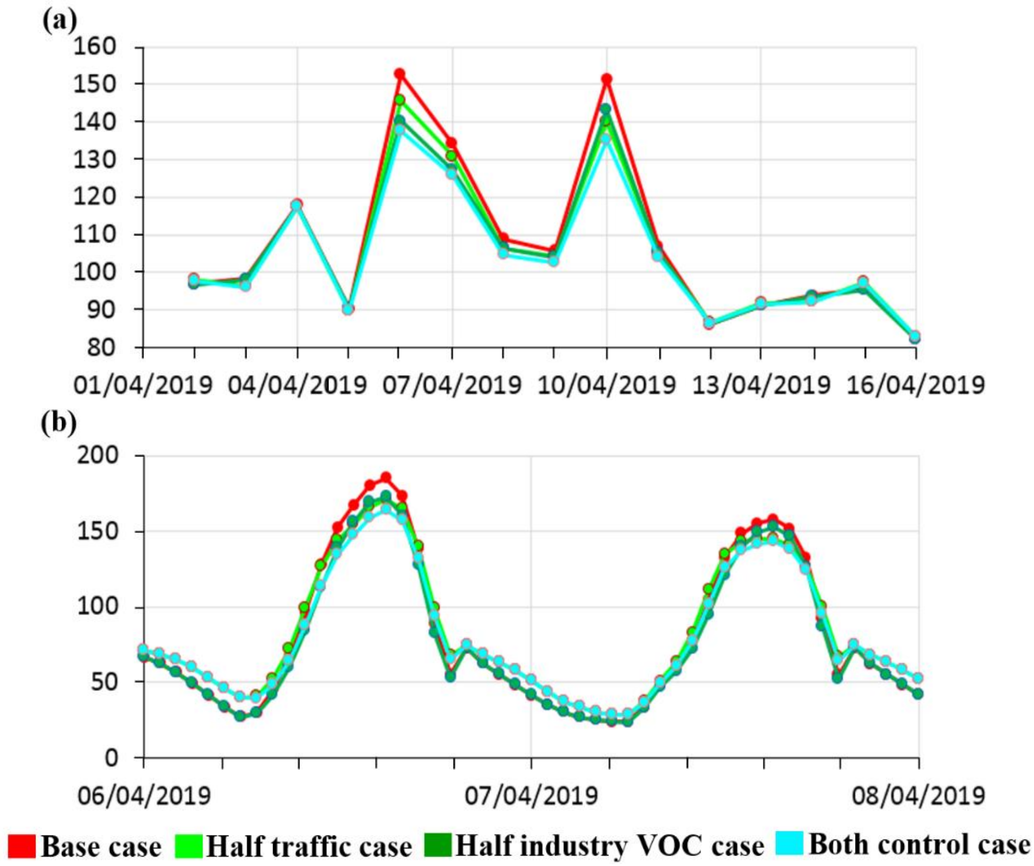
(a)
160
150
140
130
120
110
100
90
80
01/04/2019
04/04/2019
07/04/2019
10/04/2019
13/04/2019
16/04/2019
(b)
200
150
100
50
0
06/04/2019
07/04/2019
08/04/2019
Base case
Half traffic case
Half industry VOC case
Both control case